

Neural CRNs: A Natural Implementation of Learning in Chemical Reaction Networks

Rajiv Teja Nagipogu and John H. Reif*

Department of Computer Science, Duke University, 2127 Campus Drive, Durham, NC 27708

E-mail: rajivteja.nagipogu@duke.edu

Rajiv Teja Nagipogu and John H. Reif*

Department of Computer Science, Duke University, 2127 Campus Drive, Durham, NC 27708

E-mail: rajivteja.nagipogu@duke.edu

Abstract

We present Neural CRNs, an efficient, autonomous, and general-purpose implementation of learning within mass action chemical reaction systems. Unlike prior works, which transliterate discrete neural networks into chemical systems, Neural CRNs are a purely analog chemical system, which encodes neural computations in the concentration dynamics of its chemical species. Consequently, the chemical reactions in this system stay true to their nature, behaving as atomic end-to-end computational units, resulting in concise and efficient reaction network implementations. We demonstrate this efficiency by assembling a highly streamlined supervised learning procedure that requires only two clock phases. We further validate the robustness of our framework by constructing Neural CRN circuits for several linear and nonlinear regression and classification tasks. Furthermore, a minimal linear regression circuit is assembled using only 13 reactions and 15 species. Our nonlinear modeling circuits significantly advance the state-of-the-art through compact and simple implementations. The synergistic nature of our framework with the analog chemical computing hardware leaves ample room for optimizations and approximations in the computational model, several of which are discussed in this work. We believe that our work introduces a novel paradigm for chemical computing and learning, providing a foundational platform for future adaptive biochemical circuits with applications in fields, such as synthetic biology, bioengineering, and adaptive biomedicine.

Keywords: Neural CRNs, biochemical learning, chemical neural networks, molecular computing, DNA computing, chemical reaction networks

1 Introduction

Adaptive behavior is a characteristic feature of all living organisms and allows them to survive in constantly changing environments.¹ In this regard, organisms at all levels of complexity have developed *learning* mechanisms to acquire knowledge from their surroundings. In higher organisms, these mechanisms are carried out through specialized structures like the brain and the nervous system. Even without such sophistication, single-celled organisms were shown to be capable of adaptive behaviors facilitated by their internal biochemical circuitry. Examples of such behaviors include bacterial chemotaxis for finding food,² avoidance responses to unfavorable stimuli,³ and bacterial swarming to escape predation.⁴ Developing biocompatible implementations of such adaptive biochemical circuits is an important and challenging task that could potentially lead to novel applications in many fields, including biotechnology,⁵ adaptive biomedicine,^{6–8} and artificial life.⁹

The primary goal of this work is to develop a standalone implementation of *chemical learning*, i.e., learning implemented within chemical reaction networks (CRNs), with a broader goal of realizing them in synthetic biochemistries. This line of inquiry falls broadly under the ongoing investigations into biomolecular computing, which seek to create scalable and practical molecular-scale computational systems using biomolecular reaction systems (e.g., DNA strand displacement circuits).^{10–13}

Existing implementations of chemical learning primarily focus on developing chemical analogues of conventional neural networks, including McCulloch-Pitts neurons,¹⁴ Perceptrons,^{15–18} feedforward neural networks (FFNNs),^{19–22} and Boltzmann machines.²³ However, these implementations have one main drawback that their circuits are constructed by composing the chemical implementations of digital computing primitives. Such a construction necessitate “breaks” within the inherently analog computing nature of the chemical reaction systems, necessitating isolated sequential steps, which significantly increase the complexity of the reaction network implementation, in the originally intended single-pot reaction model. Furthermore, the difficulty in calculating precise gradients through backpropagation constrains many of these implementations to use first-order approximation of gradients,^{19,20} which could lead to potential

loss in circuit sensitivity and instabilities during training.

To tackle these issues, we propose *Neural CRNs*, a conceptually different approach to chemical learning, modeled as a deterministic mass action CRN system. Instead of functionally mimicking the architectures of discrete neural networks, Neural CRNs are modeled as an analog system, derived from a continuous dynamical system-based implementation of learning known as Neural Ordinary Differential Equations (Neural ODEs). Neural ODEs model neural computations using ODE evolutions of their state variables. Accordingly, the Neural CRN architecture is constructed by taking the operations in the Neural ODE architecture as a reference and functionally replicating them using CRNs. The resulting analog nature of Neural CRNs allows for several CRN-based optimizations and approximations that considerably reduce the circuit complexity, leading to concise implementations that are more practical.

The rest of the manuscript is organized as follows. First, we briefly outline the Neural ODEs framework. Then, we show the construction of the Neural CRNs framework and its novel supervised learning procedure. We then validate our framework through training and inference demonstrations on several linear and nonlinear regression and classification tasks. Then, we discuss various control parameters of the framework, possible optimizations, and simplifying assumptions that could lead to further reduction in the circuit size and complexity. Finally, we discuss the challenges involved in the practical realization of Neural CRNs and propose plausible solutions to overcome them.

2 Background

2.1 Supervised Learning in Feedforward Neural Networks

Feedforward Neural Networks (FFNNs; neural networks for short) are layered graph-like structures with directed weighted connections between nodes of neighboring layers. The weights of these connections serve as the *network parameters* and facilitate learning through gradient-based optimization methods.^{24,25} These methods “train” the network by adjusting the parameters towards optimizing an objective function, such as minimizing a risk or maximizing

a reward.

Supervised learning is one such learning approach, in which the network is optimized over a “labeled” dataset of input/output pairs. In this approach, the network is trained iteratively to learn a transformation function from the input space to the output space, such that the final transformation function can accurately predict the output corresponding to a previously unseen input.

Each iteration of supervised learning (corresponding to the input/output pair (\mathbf{x}, y)) consists of two main phases: (i) the feedforward phase and (ii) the feedback phase. Briefly, the *feedforward* phase involves computing the network output \hat{y} given \mathbf{x} by transforming it sequentially through the layers of the network according to the current parameter set. The effective computation is represented using $F_{\theta}^{\text{current}}$ as shown in eq. (1). The *feedback phase* involves computing the parameter gradients with respect to a loss function $\frac{\partial \mathcal{L}}{\partial \theta}$, where loss \mathcal{L} is defined as the error between \hat{y} and y (2). For this purpose, neural networks employ the *backpropagation* algorithm,²⁴ an efficient implementation of the chain rule for partial differentiation,²⁶ Finally, the current parameters are updated according to these gradients using the gradient descent formulation shown in eq. (3).

$$\hat{y} = F_{\theta}^{\text{current}}(\mathbf{x}) \quad (1)$$

$$\mathcal{L} = \text{error}(\hat{y}, y) \quad (2)$$

$$\theta^{\text{updated}} = \theta^{\text{current}} - \eta \frac{\partial \mathcal{L}}{\partial \theta}. \quad (3)$$

Here, η represents the learning rate that indicates how fast the network learns. This two-phase process is repeated over the entire dataset multiple times until the loss converges, after which the network is declared to be *trained* for the supervised learning task represented by the dataset. A more detailed mathematical description of the supervised learning procedure in neural networks is provided in SI Text S1.

2.2 Neural Ordinary Differential Equations

Neural ordinary differential equations (Neural ODEs)²⁷ are a continuous dynamical system-based implementation of learning and thus represent a conceptually different approach to neural computations in FFNNs. While FFNNs are discrete systems that utilize matrix transformations at discrete layers to perform the neural computations, Neural ODEs model them using the ODE evolution of their continuous state variables. These computations are then evaluated by solving the initial value problems (IVPs) of these ODE evolutions.²⁸

Figure 1 depicts the supervised learning architecture in the Neural ODEs framework. Here, we consider a supervised learning task with input $\mathbf{x} \in \mathbb{R}^n$ and the corresponding output $\mathbf{y} \in \mathbb{R}^m$. Recall that the computations in Neural ODEs are modeled as ODE evolutions, which means that they are dimension-preserving. Here, we assume that the dimensionality of the Neural ODE is d , i.e., its hidden state is a d -dimensional vector $\mathbf{z} \in \mathbb{R}^d$. Therefore, in order to align the inputs and outputs of the supervised learning task with Neural ODE dimensionality, two auxiliary linear projection layers $W_{\text{in}}^{n \times d}$ and $W_{\text{out}}^{d \times m}$ are included alongside the Neural ODE. Briefly, W_{in} effects a transformation from the input space to Neural ODE space, while W_{out} effects a transformation from Neural ODE space to the output space. Below, we describe the computations involved in the supervised learning procedure of the Neural ODEs framework. A summary of this procedure is provided in Table 1 for reference. We refer the reader to the original work²⁷ for a more detailed description.

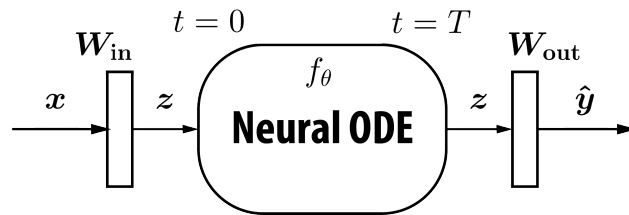


Figure 1: Schematic of the supervised learning architecture in Neural ODEs.

The feedforward phase begins at time $t = 0$ with the input \mathbf{x} being mapped into the hidden state \mathbf{z} through the input projection layer W_{in} . Then, \mathbf{z} evolves from $t = 0$ to $t = T$ following the dynamics specified by f_θ (see Table 1 for the corresponding IVP). The final evolved hidden state $\mathbf{z}(T)$ is then passed through the output projection layer W_{out} to obtain the network output

$\hat{\mathbf{y}}$. This concludes the feedforward phase.

The feedback phase begins with computing the loss \mathcal{L} between $\hat{\mathbf{y}}$ and \mathbf{y} . Instead of using the standard backpropagation algorithm like in FFNNs, which requires reverse propagating through the operations of the forward phase, the Neural ODEs framework computes loss gradients using the *adjoint sensitivity method*.²⁹ This method introduces a special *adjoint state* variable \mathbf{a} , defined as $\mathbf{a} = \frac{\partial \mathcal{L}}{\partial \mathbf{z}}$, which facilitates gradient computation by simultaneously solving three ‘backpropagation’ ODEs in reverse time (from $t = T$ to $t = 0$) to: (i) hidden state \mathbf{z} backpropagation, (ii) adjoint state \mathbf{a} backpropagation, and (iii) gradient \mathbf{g}_θ evolution. The hidden state \mathbf{z} begins at its final feedforward state $\mathbf{z}(T)$, and flows backward to its initial state $\mathbf{z}(0)$, retracing its feedforward phase trajectory. The adjoint state \mathbf{a} starts from an initial value of $\mathbf{a}(T) = \frac{\partial \mathcal{L}}{\partial \mathbf{z}}(T)$ and evolves into its final state at $t = 0$. The parameter gradients \mathbf{g}_θ start from a zero initial value at $t = T$ and evolve into their final values at $t = 0$. The simultaneous evolution of these three state variables ensures that the network evolves gradients alongside the variables it depends on, i.e., \mathbf{a} and \mathbf{z} . The gradient values at the end of backpropagation ($\mathbf{g}_\theta(0)$ at $t = 0$) are used to update the parameters according to the gradient descent formulation (3).

The analog nature of the Neural ODEs framework makes it a more suitable reference for implementing chemical learning compared to the discrete FFNNs. For instance, increasing model complexity in FFNNs requires adding additional layers, which in turn introduces additional sequential steps, making the resulting one-pot reaction network implementation more cumbersome. In contrast, depth is defined in Neural ODEs by the T parameter, meaning that increasing model complexity doesn’t require more sequential steps, but rather involves running the same step for a longer duration. Moreover, the backpropagation algorithm in FFNNs necessitates storing the activations across hidden layers for adjoint backpropagation to compute gradients, leading to a significant memory overhead. In contrast, Neural ODEs avoid this overhead by simultaneously backpropagating the hidden state alongside its adjoint state, thus requiring only constant memory.

Table 1: Supervised learning procedure in the Neural ODEs framework consisting of seven steps. Each step can be classified into a ‘discrete’ (1, 3, 4, 5, 7) or ‘analog’ (2, 6) step based on the nature of its computations. ‘Analog’ steps are marked with an asterisk (*). The discrete computations are shown as instantaneous, while analog computations take place over a time interval. Also, notice that the analog computations in step (6) take place in reverse-time.

Step	Description	Time	ODE	IVP
1	Feeding the input	$t = 0$	$z(0) = W_{\text{in}} \mathbf{x}$	
Feedforward Phase Begins				
2*	Hidden state evolution	$t = 0$ to $t = T$	$\frac{dz}{dt} = f_{\theta}(\mathbf{x}, \mathbf{z})$	$z(T) = z(0) + \int_0^T f_{\theta}(\mathbf{x}, \mathbf{z}) dt$
3	Output calculation	$t = T$	$\hat{y} = W_{\text{out}} z(T)$	
Feedforward Phase Ends; Feedback Phase Begins				
4	Loss calculation	$t = T$	$\mathcal{L} = \frac{1}{2}(\hat{y} - y)^2$	
5	Hidden state initialization	$t = T$	$z(T)$ from the feedforward phase	
	Adjoint initialization	$t = T$	$\mathbf{a}(T) \leftarrow \frac{\partial \mathcal{L}}{\partial \mathbf{z}}(T)$	
	Gradient initialization	$t = T$	$\mathbf{g}_{\theta}(T) \leftarrow \mathbf{0}$	
6*	Hidden state backpropagation	$t = T$ to $t = 0$	$\frac{dz}{dt} = f_{\theta}(\mathbf{x}, \mathbf{z})$	$z(0) = z(T) + \int_T^0 f_{\theta} dt$
	Adjoint state backpropagation	$t = T$ to $t = 0$	$\frac{d\mathbf{a}}{dt} = -\mathbf{a}^T \frac{\partial f_{\theta}}{\partial \mathbf{z}}$	$\mathbf{a}(0) = \mathbf{a}(T) + \int_T^0 -\mathbf{a}^T \frac{\partial f_{\theta}}{\partial \mathbf{z}} dt$
	Gradient evolution	$t = T$ to $t = 0$	$\frac{d\mathbf{g}_{\theta}}{dt} = -\mathbf{a}^T \frac{\partial f_{\theta}}{\partial \theta}$	$\mathbf{g}_{\theta}(0) = \mathbf{g}_{\theta}(T) + \int_T^0 -\mathbf{a}^T \frac{\partial f_{\theta}}{\partial \theta} dt$
Feedback Phase Ends				
7	Parameter update	$t = 0$	$\theta^{\text{new}} = \theta^{\text{old}} - \eta \mathbf{g}_{\theta}(0)$	

3 Results

In this section, we present the main results of this work. First, we construct a Neural CRN system for an example supervised learning task, illustrating the different CRNs involved in the training procedure. Then, we validate the constructed framework through proof-of-concept demonstrations of training and inference on several linear and nonlinear regression and classification tasks.

3.1 The Neural CRNs Framework

Construction

The Neural CRNs framework is broadly derived from the Neural ODEs framework. While the general construction process involves translating the operations in Neural ODE supervised learning process into equivalent CRNs, two main issues need to be addressed as we translate from an originally *in silico* implementation of Neural ODEs into a reaction network implementation of Neural CRNs.

The first issue relates to the choice of Neural ODE system used as the reference, which could be condensed to the choice of f_θ function. Recall that f_θ function crucially determines the ODEs in the Neural ODEs framework. In the original Neural ODEs framework, f_θ is typically chosen to be an FFNN to enable efficient computation of the Jacobians ($\frac{\partial f_\theta}{\partial \theta}$ and $\frac{\partial f_\theta}{\partial \mathbf{z}}$) using standard automatic differentiation tools.²⁶ However, the choices of f_θ are restricted while constructing a Neural CRN system. This is because the dynamics of mass action CRNs correspond to a restricted subset of polynomial ODEs known as the *kinetic differential equations* (KDEs).³⁰

Definition 1. *A kinetic differential equation is a polynomial ODE that satisfies the following requirements.*

1. *All its variables must be positive-valued.*
2. *The ODE must not have negative cross-effects, i.e., any monomial on the right-hand side*

with a negative sign must contain the differential variable also as a factor variable.

However, even if a Neural ODE is devised with a KDE f_θ system, it would require polynomial ODEs that does not satisfy the KDE restrictions (referred to as *non-KDEs*). For example, adjoint and gradient variables can sometimes take on negative values. To address this issue, non-KDEs in the parent Neural ODE are first transformed into KDEs using dual-rail encoding, before translating them into their respective CRNs^{31,32} (also see SI Text S3 for examples of such conversion). In accordance to these observations, any polynomial f_θ could be used as the dynamics function for constructing a Neural CRN system. First, all the polynomial ODEs in the expanded Neural ODE system are converted into KDEs. Then, each KDE is independently translated into a mass action CRN following the *canonic mechanism* (presented in SI Algorithm S1). Briefly, this mechanism translates each KDE monomial into a single chemical reaction, with the differential variable as the product and the monomial factor variables as the reactants. Additionally, the reaction is catalytic in its reactants. While this mechanism might not always yield the most optimal CRN, it allows for an algorithmic construction of the reaction circuits, making it well-suited for our proof-of-concept demonstrations. In future, we will explore optimizations to reduce the circuit size and develop more efficient translation frameworks.^{33,34} Additionally, note that, in canonic mechanism, the order of the KDE monomial determines the molecularity of the resulting reactions. Since implementing reactions with molecularity greater than two is challenging in chemistry, our choice of f_θ is further restricted to lower-order polynomial functions of order atmost two.

The second challenge involves translating the discrete computations in the Neural ODEs framework into the Neural CRNs framework. As shown in Table 1, while the analog ODE evolutions in the feedforward and feedback phases are the core computational aspects of the Neural ODEs framework, discrete computations in between them are necessary for switching computation in between the phases. However, discretizing computation in the single-pot reaction model of Neural CRNs would lead to a disproportionate increase in the circuit complexity that greatly diminishes the gains obtained from adopting an analog computational scheme synergistic with the underlying chemical hardware. To overcome this issue, we enforce time-scale separation between the discrete and analog computations in the circuit, ensuring that

the former runs significantly faster than the latter. Specifically, we simplify all the discrete operations to be unimolecular or annihilation reactions (see SI Text S3), and design them to operate at a higher speed compared to the analog computations (which inherently involve reactions of higher molecularity). Further details regarding the practical realization of this time-scale separation are discussed in the Discussion section.

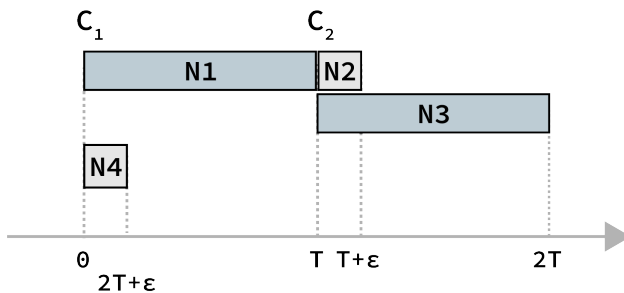


Figure 2: Arrangement of different stages in the Neural CRN supervised learning procedure on a timeline, illustrating their relative durations and the clock phases they run in.

As shown in Table 1, the supervised learning procedure in Neural ODEs is a seven-stage pipeline with ‘discrete’ and ‘analog’ stages: (1) feeding the input (discrete), (2) hidden state evolution (analog), (3) output calculation (discrete), (4) loss calculation (discrete), (5) initializing the adjoint (discrete), (6) gradient evolution (analog), and (7) parameter update (discrete). In this work, we condense this pipeline into the supervised learning procedure for Neural CRNs consisting of four stages N_1 , N_2 , N_3 , and N_4 , organized into two clock phases: C_1 and C_2 . We adopt the following strategy to achieve this reduction. First, we merge the adjacent ‘discrete’ steps into a single ‘discrete’ stage, ensuring that the pipeline alternates between ‘analog’ and ‘discrete’ stages. Next, we design each discrete stage to consist solely of unimolecular or annihilation reactions to enable time-scale separation. Accordingly, N_1 and N_3 behave as the ‘analog’ stages, while N_2 and N_4 behave as the ‘discrete’ stages. The ‘analog’ stages run for a duration of T , while time-scale separation enables the ‘discrete’ stages to run quickly within a small duration of ϵ ($\ll T$). Although a four-stage pipeline would require four clock phases for sequential execution, the fast execution of N_2 and N_4 stages allows them to overlap with their subsequent phases (N_3 , and N_1 of next iteration, respectively), thus reducing the number of required clock phases to two. Figure 2 depicts the relative durations of the stages and their arrangement on a timeline. In summary, N_1 and N_4 stages run in the C_1 phase, triggered by the

C_1 clock trigger, while N2 and N3 stages run in the C_2 phase, triggered by the C_2 clock trigger. Below, we provide a detailed description of the computations in each stage through an example Neural CRN system. Before that, we first outline several key assumptions regarding system and define the necessary translation primitives to assist in the construction.

1. To simplify the explanations, we describe the computations first in terms of algebraic variables, and provide CRN only for the final expression.
2. The ODE-to-CRN translations used to construct the Neural CRN systems in this work fall into one of the five types listed in Table 2. Their derivations are provided in SI Text S3.

Table 2: CRN translations of five prevalent polynomial ODEs in the Neural CRNs framework. A Type-I ODE only requires a single reaction. Type-II and Type-III ODEs are interpreted as a set of Type-I ODEs by rewriting them using dual-rail encoding and results in four Type-I reactions each. Type-IV results in an autocatalytic reaction. Type-V results in a decay reaction.

Type	ODE	CRN
Type-I	$\frac{dz}{dt} = xy, \quad x, y, z \in \mathbb{R}^+$	$X + Y \rightarrow Z + X + Y$
Type-II	$\frac{dz}{dt} = xy, \quad x, y, z \in \mathbb{R}$	4 Type-I reactions
Type-III	$\frac{dz}{dt} = -xy, \quad x, y, z \in \mathbb{R}$	4 Type-I reactions
Type-IV	$\frac{dz}{dt} = z^q, \quad q \in \mathbb{Z}^+, z \in \mathbb{R}^+$	$qZ \rightarrow (q + 1)Z$
Type-V	$\frac{dz}{dt} = -z^q, \quad q \in \mathbb{Z}^+, z \in \mathbb{R}^+$	$qZ \rightarrow (q - 1)Z$

3. All discrete algebraic primitives in the circuit are simplified into unimolecular transduction or annihilation reactions.
4. Algebraic variables are represented using lowercase alphabet (e.g., x), whereas the chemical species are represented using uppercase alphabet (e.g., X). Algebraic vector variables are presented as bold lowercase symbols (e.g., \boldsymbol{x}).
5. Unless explicitly stated otherwise, the chemical species are assumed to be represented in dual-rail notation, where each variable x is represented as the concentration difference between two complementary species X^+ and X^- : $x = [X^+] - [X^-]$. The \pm superscript indicates the parity of the dual-rail species.

6. Given a variable x , the corresponding dual-rail species are initialized as follows.

$$[X^+] = \max(0, x)$$

$$[X^-] = \max(0, -x).$$

A shorthand $X \leftarrow x$ is also sometimes used to represent this assignment.

7. We use shorthand expressions such as “the Z species” or “the hidden state species Z ” to collectively represent a species type and the short hand “positive (negative) Z species” to refer to the positive (negative)-parity dual-rail species of Z , respectively.
8. The hyperparameter T is a unitless quantity that represents the duration for which the CRNs in the feedforward and feedback phases are expected to run.
9. We assume the presence of a *clock mechanism* that controls the transition between sequential steps. More specifically, the dominant clock signal of a phase is expected to conditionally activate a selected set of reaction pathways corresponding to that phase, thus enabling sequential execution.

Supervised learning in the Neural CRNs framework

Here, we provide a detailed description of the supervised learning procedure in our Neural CRNs framework. For simplicity, we consider a supervised learning task with two-dimensional inputs $\mathbf{x} \in \mathbb{R}^2$ and scalar outputs $y \in \mathbb{R}$. The Neural CRN system for this task is defined with dimensionality $d = 2$ and the hidden state dynamics function:

$$f_{\theta}(\mathbf{x}, \mathbf{z}) = \theta \odot \mathbf{z} \quad \theta \in \mathbb{R}^{2 \times 1}, \mathbf{z} \in \mathbb{R}^2. \quad (4)$$

Note that these assumptions allow us to trivialize W_{in} into an identity matrix $\mathbf{I}^{2 \times 2}$, and W_{out} into a unit perceptron. Table 3 summarizes the CRNs corresponding to each stage of the supervised learning procedure, and Figure 3 provides a schematic illustration of the underlying operations and the computational flow.

Stage N1—Evolution of the hidden state species. This stage begins at time $t = 0$ with the

Table 3: Supervised learning procedure in the Neural CRNs framework. The procedure consists of four stages (N1, N2, N3, and N4) organized into two clock phases (C_1 and C_2). N1 and N3 are fast ‘discrete’ stages, while N2 and N4 are slow ‘analog’ stages. N4 and N1 run in clock phase C_1 , while N2 and N3 run in clock phase C_2 . N1 stage models the evolution of the hidden state species (Z) and runs for a duration T . N2 stage creates the adjoint species (A) and the backpropagating hidden state species (Z^b). This stage runs for a short duration ϵ ($\ll T$). N3 stage creates the gradient species G by evolving them alongside the ‘backpropagation’ CRNs of Z and A . This stage runs for a duration of T and is discussed in more detail in Table 4. N4 stage updates the parameters, flushes out the non-parametric species (Z^b, A, X), and optionally feeds the next input (X^{next}) into Z species. The parameter update reactions involve a negative feedback of G species into P species (\pm into \mp) alongside the decay of G species, simulating subtraction. The values of k_1 and k_2 are determined by the learning rate η . This stage runs for a short duration ϵ .

Stage	Phase	Expression	Name	Time	Reactions
N1	C1	$\frac{dz_i}{dt} = \theta_i z_i$	CRN _f ¹	$0 \rightarrow T$	$P_i^\pm + Z_i^\pm \rightarrow Z_i^\pm + P_i^\pm + Z_i^\pm$
N2	C2	$z_b = z$ $a = z_1 + z_2 - y$ $g_\theta = 0$ $\hat{y} = z_1 + z_2$ (optional)	CRN _b ⁰	$T \rightarrow T + \epsilon$	$Z_i^\pm \rightarrow Z_i^{b\pm} + A_1^\pm + A_2^\pm + \hat{Y}$ $Y \rightarrow A_1^\mp + A_2^\mp$ $G \leftarrow 0$
N3	C2	See Table 4	CRN _b ¹	$T \rightarrow 2T$	See Table 4
N4	C1	$\theta^{\text{new}} = \theta^{\text{old}} - \eta g_\theta$ $z = x$	CRN _b ²	$2T \rightarrow 2T + \epsilon$	$G^\pm \xrightarrow{k_1} P^\mp$ $G^\pm \xrightarrow{k_2} \Phi$ $\{Z^b, A, X\} \rightarrow \Phi$ $X^{\text{next}} \rightarrow Z$

triggering of C_1 , marking both the end of the previous supervised learning iteration and the start of the current iteration. It models the evolution of the hidden state species Z starting from an initial concentration of \boldsymbol{x} at $t = 0$ to its final concentration at $t = T$. The CRN for this phase (CRN_f^1) is described in the N1 row of Table 3. Briefly, the hidden state evolution governed by our chosen f_θ (4) results in Type-II ODEs of the form $\frac{dz_i}{dt} = \theta_i z_i$, which are translated into CRN_f^1 using the corresponding translation template from Table 2. CRN_f^1 is run until $t = T$, at which point C_2 triggers, switching the execution into N2 and N3 stages.

Stage N2—Preparing for the feedback phase. Triggered by C_1 , this stage prepares the Neural CRN system for its feedback phase. Here, we condense the three sequential ‘discrete’ steps (steps 3, 4, and 5) from Table 1 into a single discrete stage, effectively compiling their final result into three simultaneous operations: (i) creating the ‘backpropagation’ hidden state species Z^b (for hidden state backpropagation); (ii) initializing the adjoint species A (for adjoint backpropagation); and (iii) initializing the gradient species G to zero (for gradient evolution). The initialization of Z^b species occurs through unimolecular copy reactions between Z and Z^b . The expression for the adjoint species is a more involved computation; to simplify its final expression, we assume without loss of generality that the final output projection layer W_{out} is a unit perceptron and use *squared error* as the loss function \mathcal{L} (6), yielding the expression: $a = z_1 + z_2 - y$, shown in N2 row of Table 3 (full derivation provided in SI Text S3). The corresponding CRN (CRN_b^0) involves Z species positively feeding into the adjoint species A (in addition to the Z^b species) and the output species Y negatively feeding into the A species. The gradient species G are initialized to zero at the beginning of this stage. Optionally, if the system is operating in the “inference-only” mode, a network output species \hat{Y} could be generated alongside the A species. Since all the reactions involved are unimolecular, time-scale separation is enabled, ensuring that this stage runs quickly within a short duration ϵ ($\ll T$) from $t = T$ to $t = T + \epsilon$. This stage overlaps with the N3 stage, which also begins at $t = T$ with the triggering of C_2 .

$$\hat{y} = w_1 z_1 + w_2 z_2 \quad (5)$$

$$\mathcal{L} = \frac{1}{2}(\hat{y} - y)^2 \quad (6)$$

$$a_i = z_1 + z_2 - y \quad \text{using } \mathbf{a} = \frac{\partial \mathcal{L}}{\partial \mathbf{z}} \text{ and } w_i = 1 \quad (7)$$

Stage N3—Evolution of the gradient species. Similar to the N2 stage, this stage is also triggered by C_2 . The main goal of this stage is to evolve the gradient species G for updating the parameters. Recall that in the Neural ODEs framework, the gradient calculation involves simultaneously evolving three ‘backpropagation’ ODEs of \mathbf{z} , \mathbf{a} , and \mathbf{g}_θ in reverse time. Consequently, in Neural CRNs, the G species are created by simultaneously running three ‘backpropagation’ CRNs (collectively represented by CRN_b^1), corresponding to the backpropagation of Z , A , and G species. However, since CRNs are physical processes, they cannot run in the reverse time, as required by the Neural ODEs framework. Therefore, the parities of the ‘backpropagation’ ODEs are first inverted to turn them into forward-time ODEs before converting into CRNs. Table 4 outlines this translation process. The first row lists the reverse-time ODEs from the Neural ODE feedback phase. The second row shows these ODEs with inverted parities for conversion into CRNs. The third row provides their vector expressions and the fourth row enumerates their terms. The fifth row specifies the appropriate translation template for converting the ODEs from the fourth row into CRNs. The sixth row provides initial concentration assignments for the corresponding evolving species. In summary, this stage runs CRN_b^1 for a duration of T (from $t = T$ to $t = 2T$), after which C_1 phase triggers, switching the execution to N4 stage for updating the parameters. Note that C_1 also activates the N1 stage beginning a new training iteration with the next incoming input.

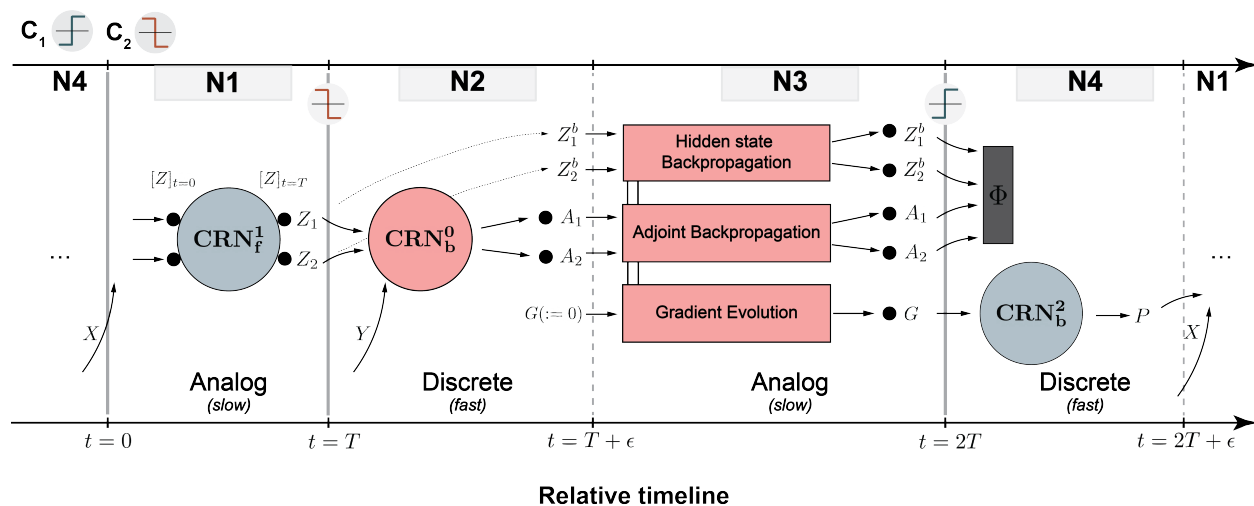
Stage N4—Updating the parameters. Triggered by C_2 , this stage updates the parameter species P using the G species created during the N3 stage. Additionally, this stage also flushes out all the non-parametric species to prepare the system for the next iteration. The gradient descent parameter update rule (see N4 stage in Table 3) involves two algebraic operations: multiplication $\Delta\theta = \eta g_\theta$ and subtraction $\theta^{\text{old}} - \Delta\theta$. The combined computation can be

Table 4: Backpropagation CRNs of the Neural CRNs framework corresponding to the backpropagation of Z and A species and the creation of G species. (Row 1) Backpropagation ODEs of the Neural ODEs framework that run in reversed time (from $t = T$ to $t = 0$). (Row 2) ODEs with their parities inverted to facilitate conversion into CRNs. (Row 3) ODE evaluation. (Row 4) Terms in the ODE expansion. (Row 5) Template from Table 2 to be applied for the ODE-to-CRN translation. (Row 6) Initialization of the evolving species.

Row	Remark	Backpropagation		
		Hidden State	Adjoint	Gradient
1	$T \rightarrow 0$	$\frac{dz}{dt} = \theta \odot z$	$\frac{da}{dt} = -\mathbf{a}^T \frac{\partial f_\theta}{\partial z}$	$\frac{d}{dt} \frac{\partial \mathcal{L}}{\partial \theta} = -\mathbf{a}^T \frac{\partial f_\theta}{\partial \theta}$
2	$0 \rightarrow T$	$\frac{dz}{dt} = -\theta \odot z$	$\frac{da}{dt} = \mathbf{a}^T \frac{\partial f_\theta}{\partial z}$	$\frac{d}{dt} \frac{\partial \mathcal{L}}{\partial \theta} = \mathbf{a}^T \frac{\partial f_\theta}{\partial \theta}$
3	Expression	$\frac{dz}{dt} = -\theta \odot z$	$\frac{da}{dt} = \mathbf{a} \odot \theta$	$\frac{d}{dt} \frac{\partial \mathcal{L}}{\partial \theta} = \mathbf{a} \odot z$
4	Expansion	$\frac{dz_i}{dt} = -\theta_i z_i$	$\frac{da_i}{dt} = a_i \theta_i$	$\frac{dq_i}{dt} = a_i z_i$
5	Translation	Type-III ODE	Type-II ODE	Type-II ODE
6	Initial concentration	$Z_{init}^b \leftarrow z(T)$	$A_{init} \leftarrow z_1 + z_2 - y$	$G_{init} \leftarrow 0$

represented using two reactions: (i) the positive (negative) G species feeding into their opposite parity P species with rate constant k_1 , and (ii) the decay of G species with rate constant k_2 . The value of η in this expression could be controlled by appropriately choosing k_1 and k_2 : $\eta = \frac{k_1}{k_1 + k_2}$ (see SI Text S3 for the derivation). Since all the reactions in this stage are unimolecular, time-scale separation can be enabled, restricting the stage to complete within a short duration $\epsilon (\ll T)$ from $t = 2T$ to $t = 2T + \epsilon$. As such, this stage overlaps with the N1 stage of the next training iteration. Apart from manipulating the η value, the learning characteristic of the network could also be modified by adjusting the runtime of the N3 stage, which indirectly controls the amount of G species formed. Optionally, this stage can involve copying the input species of the next iteration (X^{next}) into the Z species. Note that to avoid conflict between this step and the flushing out operation of the current iteration's Z , the feedforward phase's Z species are preemptively copied into the Z^b species during the N2 stage, and the backpropagation is performed on the Z^b species.

Figure 3: A schematic of the Neural CRN training procedure depicting the flow of information. Each training iteration consists of four stages N1, N2, N3, and N4 separated by two clock triggers C_1 and C_2 . Time-scale separation is enforced to separate them into slow ‘analog’ and fast ‘discrete’ stages. The ‘dashed’ line in the right edge of a panel signifies that the corresponding stage overlaps runs in conjunction (albeit for a short duration ϵ) with its adjacent stage. At time $t = 0$ N1 begins with its Z species initialized with input species X , which then evolve until $t = T$ according to CRN_f^1 . At $t = T$, the C_2 phase is triggered, which starts both N2 and N3 stages. N2 creates the adjoint species A and hidden state backpropagation species Z^b by running CRN_b^0 . This stage lasts for a short duration till $t = T + \epsilon$. N3 stage simultaneously executes the three backpropagation CRNs of Z^b , A , and G species and runs for a duration of T until $t = 2T$. At $t = 2T$, C_1 triggers, switching the execution to both N1 and N4 stages. N4 stage uses the G species from the end of N3 stage to update the parameter species P by running CRN_b^2 for a short duration ϵ till $t = 2T + \epsilon$. Note that this phase overlaps with the N1 stage of the next iteration.



3.2 Neural CRNs for Linear Regression

Linear regression is a supervised learning task in which the output is modeled as a linear transformation of the input. Here, we utilize the construction framework discussed above to develop a Neural CRN system capable of learning linear regression tasks, named the *Linear Regressor Neural CRN* (LR-NCRN). An additional goal of this construction is to showcase a minimal-size chemical learning circuit achievable using the Neural CRNs framework.

LinReg2D: *LinReg2D* is a linear regression task with positive-valued inputs $\mathbf{x} \in \mathbb{R}_{>0}^2$ and a positive scalar output $y \in \mathbb{R}_{>0}$. The dataset for this task is created by independently sampling the inputs from the uniform distribution $\mathbf{x} \sim \mathcal{U}(1.0, 5.0)$ (limits chosen arbitrarily) and the corresponding outputs assigned using the formula

$$y = k_1x_1 + k_2x_2 + k_0 + \xi \quad (8)$$

where ξ represents Gaussian noise modeled as $\xi \sim \mathcal{N}(0.0, 0.4)$. The hyperparameters are arbitrarily as follows: $k_1 = 1$, $k_2 = 2$, and $k_0 = 1.0$.

The LR-NCRN is defined with dimensionality $d = 2$ and hidden state dynamics function

$$f_{\theta}^{\text{linreg}} = \theta \odot \mathbf{x} + \beta \quad (9)$$

where $\theta \in \mathbb{R}_{>0}^2$ and the bias $\beta \in \mathbb{R}_{>0}$. The LinReg2D task is designed with positive-valued inputs and outputs so that the variables θ and z can remain positive throughout the training process, which allows them to be specified in single-rail notation. Consequently, only the gradient species G and the adjoint species A need to be specified in dual-rail notation. Additionally, the hyperparameter T is chosen carefully to prevent θ from becoming negative, ensuring that the single-rail specifications of P and Z species remain valid throughout the training process.

Table 5 presents the CRNs from each stage of the supervised learning procedure in the LR-NCRN circuit. The N1 stage modeling the hidden state evolution requires two Type-I ODEs due to the $\theta_i x_i$ term and one unimolecular transduction reaction due to the β term. The N2 stage modeling adjoint calculation, requires three reactions with the two Z species feeding

positively and one Y species feeding negatively into the A species. The N3 stage, which typically requires running three backpropagation CRNs, only needs to run the CRN for the evolution of G species. This is because, the lack of the z term in $f_{\theta}^{\text{linreg}}$ avoids running the ‘backpropagation’ CRN of A species (since $\frac{\partial f_{\theta}}{\partial z} = 0$, adjoint backpropagation is nullified; see the ‘Adjoint’ column in Table 4), while the lack of the z -term in the gradient dynamics expression avoids the ‘backpropagation’ CRN of Z species. The resulting circuit consists of two Type-II ODEs and requires four reactions (instead of eight, since x is positive-valued). The N4 stage updating the parameter species involves negative G species increasing (through positive feedback), and positive G species decreasing (through annihilation) the amount of P species. The resulting circuit requires four reactions, two per each P_i . Overall the circuit requires 17 species and 14 reactions. Optionally, the circuit also requires to flush out the A and X species at the end of each iteration. More details regarding the implementation of this circuit are provided in SI Text S4.

Table 5: The Linear Regressor Neural CRN (LR-NCRN) circuit designed for the LinReg2D task ($i = \{1, 2\}$). (*left*) Species of the circuit. Since the task features positive-valued inputs and outputs, only A and G are required to be in dual-rail notation. Rest of the species are specified in single-rail notation. The circuit requires 17 species in total. (*right*) Reactions in the resulting circuit. N1 stage involves three reactions with two Type-I ODEs and one bias term. N2 stage involves three reactions with two Z species positively feeding and one Y species negatively feeding into the A species. N3 stage only involves only gradient evolution (the other two ‘backpropagation’ CRNs can be ignored) resulting in four reactions. N4 stage involves negative feedback from G species resulting in four reactions. Optionally at the end, the non-parametric species should be flushed out, preparing for the next iteration. The resulting circuit involves 14 reactions in total (excluding the flushing reactions at the end).

Group name	Species	Stage	ODE	Reactions
Inputs	X_1, X_2	N1	$\frac{dz_i}{dt} = \theta_i x_i + \beta$	$X_i + P_i \rightarrow Z_i + X_i + P_i$ $B \rightarrow Z_1 + Z_2$
Output	Y	N2	$a_i = z_1 + z_2 - y$	$Z_i \rightarrow A_1^+ + A_2^+$ $Y \rightarrow A_1^- + A_2^-$
Parameters	P_1, P_2	N3	$\frac{dg_i}{dt} = a_i x_i$	$X_i + A_i^{\pm} \rightarrow G_i^{\pm} + X_i + A_i^{\pm}$
States	Z_1, Z_2	N4	$\theta_i = \theta_i - g_i$	$G_i^- \rightarrow P_i$ $G_i^+ + P_i \rightarrow \Phi$
Adjoints	A_1^{\pm}, A_2^{\pm}	Total		14
Gradients	G_1^{\pm}, G_2^{\pm}	Flushing at iteration end		$\{A_i^{\pm}, X_i\} \rightarrow \phi$
Clock signals	C_1, C_2			
Total	17			

Figure 4 depicts the results of training and inference for the LR-NCRN circuit on the LinReg2D task. Figure 4a shows the training set with the data points (x_1, x_2, y) scattered on the

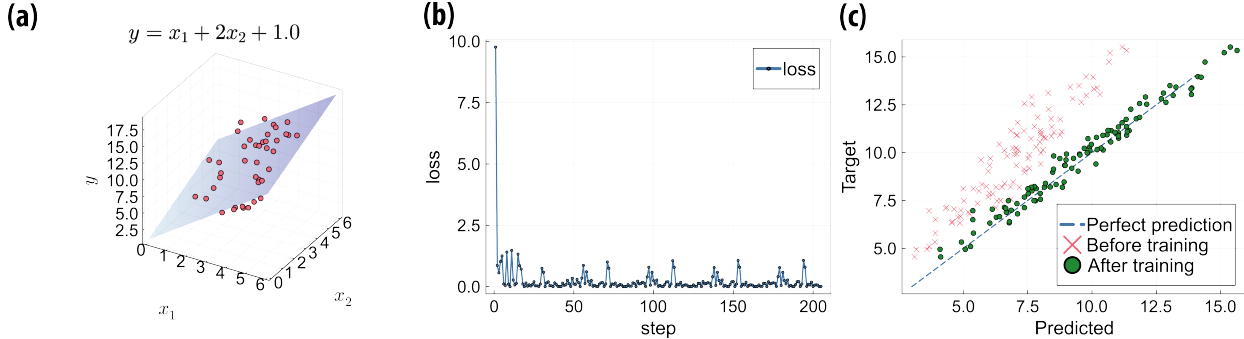


Figure 4: Results of training and inference of the Linear Regressor Neural CRN (LR-NCRN) on a linear regression task. (a) The training dataset juxtaposed with the output surface: $y = k_1x_1 + k_2x_2 + k_0$, with $k_1 = 1.0$, $k_2 = 2.0$, and $k_0 = 1.0$. (b) Step-wise loss at each iteration during training depicting loss convergence. (c) A comparison of predicted outputs on the test set against the target outputs before and after training. The data points after training are closer to the “perfect prediction line” (on which predicted = target) demonstrating the ability of our Linear Regressor Neural CRN to model linear regression tasks.

3D plane, juxtaposed with the surface plane $g(x_1, x_2) = k_1x_1 + k_2x_2 + k_0$. Figure 4b shows the loss trends after each step, demonstrating loss convergence on the training data. Figure 4c compares the (predicted, target) points before and after training, plotting them against the “perfect prediction line” (on which prediction = target). Here, we observe that predictions correlate more closely with the targets after training than before, confirming that our LR-NCRN model is capable of learning linear regression tasks.

A minimal learning circuit in the Neural CRNs framework. The LR-NCRN circuit described in Table 5 can be further simplified to form a minimal learning circuit. To achieve this, we consider a linear regression task without the bias term. This allows for the removal of the bias term from the corresponding f_θ and eliminates ‘bias’ reactions from the LR-NCRN circuit. Furthermore, both adjoint variables a_i are identical and static, allowing us to condense the four adjoint species A_i^\pm into two adjoint species A^\pm , common to both gradients. These optimizations reduce the circuit size to 13 reactions involving 15 species.

3.3 Neural CRN for nonlinear regression

Nonlinear regression is a supervised learning task in which the output is defined as a nonlinear transformation of the input. Here, we develop a Neural CRN system capable of learning nonlinear regression tasks, named the *Nonlinear Regressor Neural CRN* (NLR-NCRN). We

additionally utilize this section to describe the modifications required to extend the Neural CRNs framework to handle nonlinear modeling tasks.

NonLinReg2D. *NonLinReg2D* is a two-dimensional nonlinear regression task (NonLin-Reg2D) with inputs $x \in \mathbb{R}^2$ sampled from the uniform distribution $x \sim \mathcal{U}(0.5, 2.0)$ and the corresponding outputs assigned using the function

$$y = x_1x_2 + x_2^2 + \xi \tag{10}$$

where $\xi \sim \mathcal{N}(0, 0.1)$ represents the Gaussian noise.

Nonlinear modeling in the Neural ODEs (and by extension in Neural CRNs) is a slightly involved process. Recall that in FFNNs, nonlinear tasks are modeled by employing nonlinear “activation” functions such as ReLU or Tanh in their hidden layers. On the other hand, computations in Neural ODEs are modeled as homeomorphic flow trajectories,^{27,35} Furthermore, trajectories of different inputs cannot intersect due to the uniqueness property of ODE evolution.³⁶ Consequently, ‘vanilla’ Neural ODEs struggle with learning nonlinear tasks, as the network struggles to find the correct set of parameters that result in non-intersecting flow trajectories that can accurately represent the input/output relationships in the dataset. For example, in the ‘Rings2D’ classification task discussed in Section 3.4, the network aims to find non-intersecting flow trajectories that can spatially separate the two rings into becoming linearly separable.

To address this issue, Neural ODEs incorporate a well-known machine learning trick called *implicit lifting* or *augmenting*³⁷ into their architecture. In this technique, inputs of a nonlinear modeling task are transformed into a higher-dimensional space via a nonlinear transformation, converting the task into a linear one in this higher-dimensional space. For instance, in the ‘Rings2D’ task (see Section 3.4), a hypothetical nonlinear transformation from the 2D input space into 3D space might involve pushing the inner ring points up along the z-axis and the outer ring points down the z-axis (see SI Text S13 for a simple visualization of implicit lifting). In Neural ODEs, the augmenting process involves two key modifications to the system architecture:³⁵ (i) using a nonlinear hidden state dynamics function, and (ii) padding the inputs

with p additional dimensions. Together, these two modifications achieve the required effect of nonlinear transformation into a higher-dimensional space. Finally, the linear output projection layer W_{out} can model the resulting linear task. We refer the reader to the original work³⁵ on “augmenting” Neural ODEs for a more detailed description of the process.

We adopt this technique into the Neural CRNs framework in a similar manner: (i) by incorporating additional “padded” input species initialized to a non-zero concentration and (ii) using a nonlinear hidden state dynamics function with adjusted dimensionality. Here, we model the NLR-NCRN circuit for the NonLinReg2D task as a $d + p$ -dimensional Neural CRN circuit with $d = 2$, $p = 1$ and the required nonlinear hidden state dynamics function defined as a quadratic polynomial ODE:

$$f_{\theta}^{\text{nlreg}} = \theta \odot \mathbf{x} - \mathbf{z} \odot \mathbf{z} \quad (11)$$

where $\mathbf{x} \in \mathbb{R}^{d+p}$, $\theta \in \mathbb{R}^{d+p}$, and $\mathbf{z} \in \mathbb{R}^{d+p}$. More implementation details regarding this construction are described in SI Text S5. Note that, the dynamics function is heuristically chosen and more theoretical exploration is required to understand its dynamics and approximation capabilities.

Figure 5a shows the training dataset of the NonLinReg2D task juxtaposed against the surface plot: $y = x_1x_2 + x_2^2$. Figure 5b shows the loss progression at each iteration of the supervised learning process, demonstrating loss convergence. Figure 5c compares the (predicted, target) points before and after training, plotting them against the “perfect prediction line” (on which prediction = target). Here, we observe that predictions correlate more closely with the targets after training than before, showing that our NLR-NCRN circuit can successfully learn nonlinear regression tasks. To further demonstrate its versatility, we validate the NLR-NCRN on another nonlinear regression task: $y = \sin(x_1) + x_2^2$ in SI Text S5.2.

First-order approximation of gradients. The presence of the \mathbf{z} -term in the dynamics function $f_{\theta}^{\text{nlreg}}$ could pose a potential issue during training, as reversing the parity of f_{θ} during the feedback phase (see Table 4) leads to the presence of autocatalytic reactions in the backpropagation CRNs of both Z and A species. While the uncontrolled growth due to these

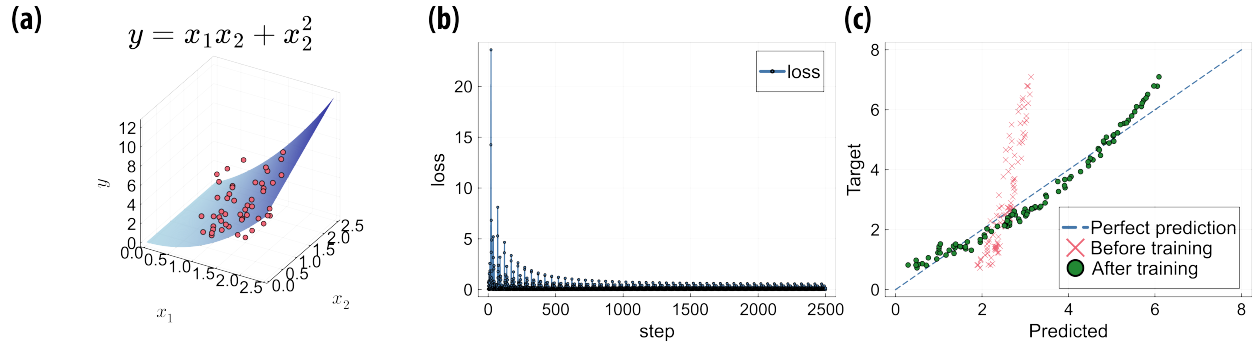


Figure 5: Results of training and inference of the NLR-NCRN model on a nonlinear regression task. (a) The training dataset juxtaposed against the output surface: $y = x_1x_2 + x_2^2$. (b) Step-wise loss at each iteration during training depicting loss convergence. (c) Comparison of predicted outputs on the test set against the target outputs before and after training. The data points after training are closer to the “perfect prediction line” (on which predicted = target) demonstrating the ability of our NLR-NCRN circuit to model linear regression tasks.

reactions could be subdued by modulating their growth rate (via a coefficient $\alpha < 1$ on the z -term) or through adjusting the runtime parameter T , any imperfections in other parts of the circuit could still cause instabilities by indirectly affecting these autocatalytic reactions. To mitigate this risk, we propose the following simplification: instead of backpropagating the adjoint species, we assume that their concentrations remain constant throughout the feedback phase. Then, by substituting the initial value of the adjoints ($a_i = z_1 + z_2 - y$; see N2 from Table 3) into the gradient evolution ODE: $\frac{dg_i}{dt} = a_i x_i$, the final value of the gradient becomes $g_i = T a_i x_i$. Notice that this expression looks similar to the perceptron weight-update rule ($\Delta w = \alpha(\hat{y} - y)x_i$; recall from eq. (7) that $a_i = \hat{y} - y$).³⁸ We demonstrate the validity of this reduced circuit by showing that it can successfully learn the NonLinReg2D task in SI Text S5.1.

3.4 Neural CRNs for Binary Classification

The regression framework of Neural CRNs can be adapted for binary classification by using real-valued class labels y^{ON} and y^{OFF} , to represent the ON and OFF classes. The network output \hat{y} is converted into a class assignment by comparing it with a predefined threshold ϕ :

$$\text{predicted class label} = \begin{cases} \text{ON} & \hat{y} > \phi \\ \text{OFF} & \text{otherwise} \end{cases} \quad (12)$$

with $y^{\text{OFF}} < \phi < y^{\text{ON}}$. However, this formulation introduces an additional design constraint that the outputs of the binary classifier Neural CRNs are expected to be within the range of $y^{\text{OFF}} \leq \hat{y} \leq y^{\text{ON}}$.

Here, we describe Neural CRNs for both linear and nonlinear binary classification tasks. The *Linear Classifier Neural CRN* (LC-NCRN) utilizes the hidden state dynamics function $f_{\theta, \beta}^{\text{lincls}}$ and is used for linear classification, while the *Nonlinear Classifier Neural CRN* (NLC-NCRN) employs $f_{\theta}^{\text{nlcls}}$ and is used for nonlinear classification. The dynamics functions for the two are defined as follows:

$$f_{\theta, \beta}^{\text{lincls}}(\mathbf{x}, \mathbf{z}) = \theta \odot \mathbf{x} + \beta \quad (13)$$

$$f_{\theta, \beta}^{\text{nlcls}}(\mathbf{x}, \mathbf{z}) = \theta \mathbf{x} + \beta - \mathbf{z} \odot \mathbf{z} \odot \mathbf{z}. \quad (14)$$

At the end of the feedforward phase, the LC-NCRN mimics the output of a linear perceptron scaled by a value of T ($\hat{y}^{\text{lincls}} = T(\theta \odot \mathbf{x} + \beta)$), whereas the NLC-NCRN approximates a three-layer FFNN with *cube root* activation function in the hidden layer, i.e., $\mathbf{z}_{ss} = \sqrt[3]{\theta \mathbf{x} + \beta}$ (recall that $\theta \mathbf{x} + \beta$ is equivalent to a simple input-weight multiplication at the hidden layer of a linear neural network). The steady state convergence and the gradient smoothness of $f_{\theta, \beta}^{\text{nlcls}}$ function are discussed in SI Text S6 and the effect of applying the cube root activation in the hidden layer on the output is depicted in SI Figure S4.

Below, we discuss the results of training and inference of these two Neural CRN classifiers on various linear and nonlinear binary classification tasks. Similar to the nonlinear regression tasks, implicit lifting trick is incorporated into the classifiers by augmenting the dimensionality of each task. We present further discussion on the circuit construction and additional simulations in SI Text S7.

Linear2D. Linear2D is a synthetic linear binary classification dataset. The inputs $\mathbf{x} \in \mathbb{R}^2$ are sampled from the uniform distribution $\mathbf{x} \sim \text{Uniform}(0, 2)$. The class labels are assigned using the discriminant function $g(x_1, x_2) = k_1 x_1 + k_2 x_2$ and a threshold ϕ (Figure 6a). The classes are equally sized. The hyperparameters are arbitrarily chosen to be: $k_1 = 1.0$, $k_2 = 2.0$, $y^{\text{ON}} = 4$, $y^{\text{OFF}} = 0$, and $\phi = 2$. Briefly, the class labels are assigned to the data points based

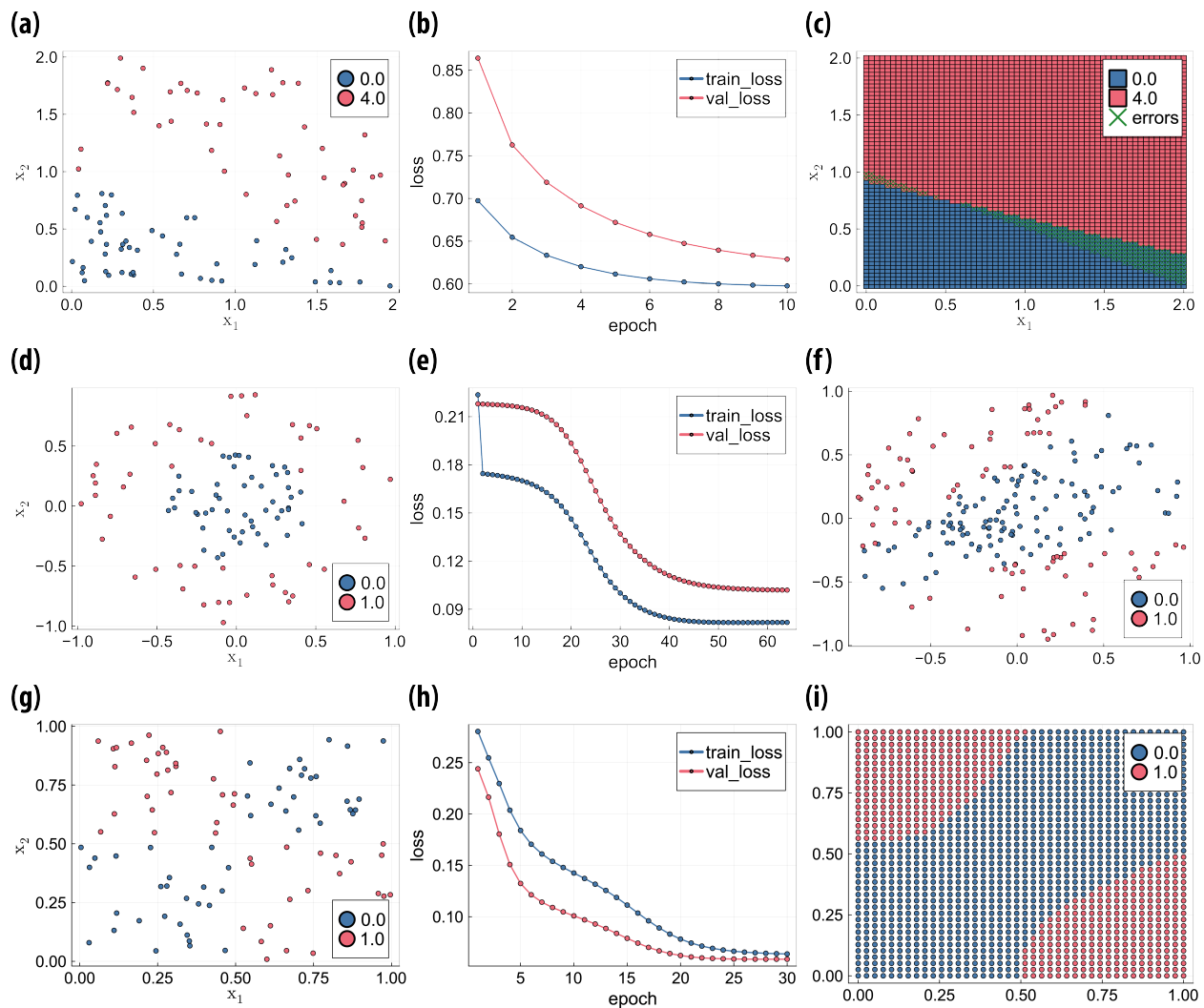


Figure 6: Results of training and inference of the Neural CRN classifiers on (a, b, c) Linear2D, (d, e, f) Rings2D, and (g, h, i) XOR tasks. The first column represents the training datasets of each task. The second column represents the loss curves on training and validation sets showing loss convergence on all three tasks. The third column shows the decision boundaries formed by the trained model on the test set.

on the relative value of the discriminant function at that point with respect to ϕ as shown below.

$$y = \begin{cases} y^{\text{ON}} & k_1x_1 + k_2x_2 > \phi \\ y^{\text{OFF}} & \text{otherwise} \end{cases}$$

Figure 6a shows the training dataset showing the distribution of points among the two classes. Figure 6b depicts the loss curves on both training and validation datasets demonstrating loss convergence. Figure 6c shows the predictions of the trained model on the test set generated as a 2D grid of uniformly spaced points, showing the learned separation boundary and the misclassified examples (marked with an \times). We observe that the separation boundary successfully approximates intended discriminant function $g(x_1, x_2) = \phi$ (from the intercepts on (a) x_2 -axis: at $x_1 = 0.0$, $x_2 \approx 1.0$ and (b) x_1 -axis: at $x_2 = 0.0$, $x_1 \approx 2.0$).

Rings2D. Rings2D is a synthetic two-dimensional binary classification dataset with the linearly inseparable (but nonlinearly separable) classes arranged in concentric ring-shaped regions centered at the origin. The inputs $\mathbf{x} \in \mathbb{R}^2$ are sampled from the uniform distribution $\mathbf{x} \sim \text{Uniform}(-1, 1)$ (Figure 6d). The classes are equally sized. The class label y for each input \mathbf{x} is assigned based on its distance from the origin using three radius hyperparameters $r_1, r_2, r_3 \in \mathbb{R}^+$ ($r_1 < r_2 < r_3$) as follows

$$y = \begin{cases} y^{\text{OFF}} & \text{if } 0 < \|\mathbf{x}\|_2 < r_1 \\ y^{\text{ON}} & \text{if } r_2 < \|\mathbf{x}\|_2 < r_3 \end{cases}.$$

The classes are equally sized. The values of the hyperparameters are chosen arbitrarily as follows: $r_1 = 0.45$, $r_2 = 0.5$, and $r_3 = 1$, $y^{\text{ON}} = 1$, $y^{\text{OFF}} = 0$. The classification threshold is set to $\phi = 0.5$.

Figure 6d shows the training set, highlighting the concentric ring structure of the dataset. Figure 6e shows the loss convergence on the training and validation datasets. Figure 6f presents the model predictions on the test set with the misclassified samples marked by an \times . Both these results confirm that the learned model was able to approximate the nonlinear separation boundary between the two classes.

XOR2D. XOR2D is another synthetic two-dimensional binary classification dataset with nonlinearly separable classes. The inputs $\mathbf{x} \in \mathbb{R}^2$ are sampled from the uniform distribution $\mathbf{x} \sim \text{Uniform}(0, 1)$. The class labels are assigned by Booleanizing the inputs (15) and applying the Boolean XOR function on these ‘Boolean’ variables as shown in eq. (16). The threshold for Booleanizing is set to $\phi^b = 0.5$.

$$x_i^b = \begin{cases} y^{\text{ON}}, & \text{if } x_i > \phi^b \\ y^{\text{OFF}}, & \text{otherwise} \end{cases} \quad (15)$$

$$y = \text{XOR}(x_1^b, x_2^b). \quad (16)$$

The hyperparameters for the classification task are set as follows: $y^{\text{ON}} = 1$, $y^{\text{OFF}} = 0$, and $\phi = 0.5$.

Figure 6g shows the training dataset depicting the spatial arrangement of the two classes in diagonal quadrants. Figure 6h shows the loss curves on the training and validation datasets depicting the loss convergence. Figure 6i qualitatively depicts the separation boundaries learned by the model for the three datasets using a uniformly spaced grid of test data points. The obtained separation boundaries correctly approximate the expected decision boundary of XOR, further validating our construction. More experiments on binary nonlinear classification are shown in SI Figure S5.

The function $f_{\theta}^{\text{nlcls}}$ being a cubic polynomial presents an implementation challenge for classification tasks, as the resulting Neural CRN would require trimolecular reactions, which are hard to implement in practice. To our best knowledge, the only other work³⁹ that presented an analog chemical implementation of a nonlinear neural network, also required trimolecular reactions. Note that there were other implementations of neural networks that only required bimolecular interactions but they are discrete cascaded architectures.^{20–22} To address the challenge of trimolecular reactions in this work, we propose a modified dynamics function that

supplants the cubic term in $f_{\theta}^{\text{nlcls}}$ with a quadratic term

$$f_{\theta}^{\text{nlclsV2}} = \theta \mathbf{x} - \alpha \mathbf{z} \odot \mathbf{z} \quad (17)$$

where α is heuristically chosen to be $\alpha = 0.3$. The inclusion of the α coefficient is intended to help balance the growth rate of different terms in the $f_{\theta}^{\text{nlclsV2}}$ function. We provide further discussion of this choice in the Discussion section and demonstrate classification performance of the Neural CRN using $f_{\theta}^{\text{nlclsV2}}$ in SI Text S8. This modification serves as a preliminary heuristic abstraction to show that nonlinear classification tasks can be learned by a Neural CRN using bimolecular reactions (since quadratic polynomial f_{θ}) as the highest-order reactions. In future work, we aim to develop a more rigorous theoretical framework to guide an informed design of f_{θ} .

4 Discussion

Neural CRNs are a general-purpose chemical learning framework that encodes neural computations within the concentration dynamics of a deterministic mass action CRN system. Consequently, in this framework, chemical reactions behave as atomic end-to-end computational units, leveraging their intrinsically analog nature. Such a synergy between the chemical reaction “software” and the underlying mass action kinetic “hardware” enables numerous approximations and optimizations, resulting in concise and efficient circuits that are amenable for a practical implementation. This efficiency is demonstrated through the development of a streamlined supervised learning pipeline that requires only two clock phases (a minimal requirement for supervised learning). Additionally, several efficient and novel “learning” circuits for linear and nonlinear regression and classification tasks are also presented.

The Neural CRN architecture, and by extension, its modeling capacity, are primarily determined by the choice of its dynamics function f_{θ} . For the construction to be feasible, f_{θ} should be a polynomial ODE. Although, for the construction to be practical, f_{θ} should be a lower-order polynomial ODE. In this work, we introduced several novel f_{θ} functions for

both linear and nonlinear supervised learning tasks. Currently, no comprehensive theory exists for selecting an appropriate f_θ for a given task. However, a prior work³⁹ has developed a mathematical framework for mass action ODEs that approximate neural network computations at steady state and analyzed their convergence properties. This work also presented mass action ODE system capable of approximating a three-layer ReLU-activated neural network (see SI Text S11). Similarly, another study²⁰ presented a CRN that models a Tanh-activated neural network at steady state. Although our nonlinear f_θ functions exhibit convergence properties (see SI Text S6), we primarily operate Neural CRNs in the pre-convergence regime, i.e., rather than focusing on the end point computation at steady state, we place more emphasis on the system dynamics effecting a nonlinear transformation on the inputs.

Supervised learning is an inherently iterative procedure with each iteration involving multiple sequential stages. Accomplishing serialization of reaction pathways is hard to achieve in a one-pot reaction model, as it leads to cumbersome and complicated reaction network implementations. In this regard, the general suggested strategy is to incorporate an oscillatory circuit as a “clock mechanism”, such that the dominant signal of each clock phase activates or inhibits a specific set of reaction pathways, either as catalysts^{40,41} or as external agents.¹⁴ However, the implementation of oscillators is a significant challenge for current molecular computing technologies (e.g., DNA strand displacement) as leakage errors in them grow uncontrollably due to their autocatalytic nature.^{42,43} To tentatively address this issue, an alternative sequential execution strategy using a microfluidic device that periodically releases clock signals was suggested.²⁰ An asynchronous implementation of chemical neural networks such as the work on Chemical Boltzmann Machines²³ requires reactions of high-molecularity, while a fully sequential implementation such as the *WP-Tanh* framework²⁰ (a Tanh-activated neural network that learns via the weight-perturbation algorithm⁴⁴) requires too many clock phases and large circuits. In contrast, our Neural CRNs approach strikes a highly efficient middle-ground, fitting the entire supervised learning into two clock phases (the minimum required), while relying solely on unimolecular and bimolecular reactions.

Beyond the time-scale separation described earlier, the analog nature of the Neural CRNs could enable additional forms of asynchronous execution. Notice that Z and A are the only

common species between the N1 and N2 stages in the feedforward phase, and N3 and N4 from the feedback phase. The Z species are already being copied into Z^b species during the N2 phase. Similarly creating a ‘backpropagation’ copy of A species fully isolates the N1, N2 and N3, N4 stages, thereby allowing the N3, N4 stages from the current iteration to run alongside the N1, N2 stages of the next iteration. While this asynchronous execution alone doesn’t fully eschew the requirement of the clock mechanism, further modifications to this framework might allow us to do so (e.g., modeling forward phase as a steady state system).

Furthermore, the parameter update stage N4 could be completely decoupled from the learning procedure by accumulating gradients over multiple iterations and executing the parameter updates after the entire training set is processed, a mechanism known as *batch gradient descent*⁴⁵ in the machine learning literature. Finally, when adapting a pre-trained network to a niche environment, a more chemically aligned learning scheme could be to train the circuit repeatedly on the same input till convergence before moving on to the next input, rather than iterating over the dataset multiple times. We will explore these possibilities in future work.

The hyperparameters that need to be adjusted while implementing a Neural CRN system include: the dimensionality d , the dynamics function f_θ , and the runtime of the ‘analog’ stages T . Typically, the value of d is chosen to be same as the input dimensionality, so as to avoid the use of W_{in} layer. However, in case of larger input dimensions, the use of W_{in} could be unavoidable ($z(0) = W_{in}x$). The selection of f_θ is perhaps the most crucial and most difficult design decision. Specifically, the presence of a z -term in the expression of f_θ could lead to autocatalytic reactions, which may cause instabilities during training if the growth rates of different terms in the f_θ expressions are skewed. Preliminary demonstration of this was obtained through the choice of $f_{\theta,\alpha}^{nclsV2}$ (17), where an additional hyperparameter α (heuristically determined) was added to the quadratic z -term to counterbalance the skew in its growth rate compared to the θx term. Finally, the parameter T is analogous to the depth parameter (number of hidden layers) in neural networks and determines the duration for which the state variable ODEs are evolved. This parameter should be tuned alongside f_θ while being cognizant of the latter’s growth rate. A low T value might result in the underexpression of nonlinearity in the dynamics function, whereas a high T value might lead to vanishing or

exploding gradients (due to the presence of autocatalytic elements in f_θ). In addition to these parameters, the $y^{\text{ON/OFF}}$ values in classification tasks and the learning rate η could be used to control the speed at which the network learns. Another hyperparameter of note is ϵ , the runtime of the ‘discrete’ stages. The relative value of ϵ is primarily dependent on the relative rates of the fast ‘discrete’ and slow ‘analog’ reactions. Considering DNA strand displacement as the framework for in vitro implementation, the limitations on the maximum strand displacement rate constant⁴⁶ and the cascaded nature of multimolecular reaction circuits,^{43,46,47} the relative durations of unimolecular and multimolecular reactions could be designed to differ by several orders of magnitude.

How does the Neural CRNs framework compare with the existing chemical neural network (CheNN) implementations in terms of circuit size and complexity? We provide qualitative comparisons between both linear and nonlinear models. For linear modeling, we compare the LR-NCRN system with the Analog Asymmetric Signal Perceptron (AASP)¹⁶ model. Both these circuits can model linear regression tasks of the form: $y = k_1x_1 + k_2x_2 + k_0$. However, note that the sizes of these two circuits cannot be directly compared as the AASP model uses an asymmetric representation, while the LR-NCRN uses a symmetric dual-rail representation. Although, a comparison could be drawn when discussed in the context of modeling positive-valued functions. The AASP circuit consists of 17 species and 18 reactions, whereas the LR-NCRN circuit requires 17 species and 14 reactions (excluding the flushing reactions at the end for a fair comparison). While the two circuit sizes are comparable, there are several implementation differences. The main difference arises from the discrete nature of the circuit. The AASP circuit while using efficient implementations of input-weight integration and parameter updates, requires the computations to occur sequentially, resulting in an increased circuit complexity. Furthermore, the circuit incurs significant design overhead due to slightly more complicated reaction circuits that require controlled reaction rates. In contrast, our Neural CRNs framework only requires two clock phases per learning iteration and the reactions have uniform rate constants.

The disparity is more conspicuous in the case of nonlinear modeling. Here, we compare our NLR-NCRN system with a hybrid model that combines the characteristics of two CheNN

implementations: (a) a non-competitive CRN (NC-CRN)-based implementation of a ReLU-activated network (NC-ReLU; for the feedforward phase),²² and (b) a Tanh-activated network that uses weight-perturbation algorithm for learning (WP-Tanh).²⁰ Both models simulate a two-input three-layer neural network with the corresponding activation function in the hidden layer. The presence of a nonlinear activation function in the hidden layer requires the NC-ReLU framework to fully compute the hidden layer activations before proceeding to the final layer, thereby requiring an additional break in the computation, which significantly increases the circuit size and complexity. Furthermore, the difficulty of calculating precise gradients forces CheNNs to use approximations like the weight-perturbation algorithm⁴⁴ in the WP-Tanh model: $\frac{\partial \mathcal{L}}{\partial w_i} \approx \frac{\mathcal{L}(w_i + \Delta w_i) - \mathcal{L}(w_i)}{\Delta w_i}$. This algorithm updates each weight independently, requiring multiple clock cycles per learning iteration. Such independent weight-updates may also trap the network in sub-optimal local minima,²⁰ which derails the training process. While a parallelized version of the weight-perturbation algorithm could update all the weights simultaneously, it would require a prohibitively large circuit. In contrast, our Neural CRNs framework calculates all the parameter gradients simultaneously by just running three ‘backpropagation’ CRNs. Although implicit lifting increases circuit size, this can potentially be mitigated by sparsifying the parameter matrix θ_{sparse} through a static version of dropout,⁴⁸ a common approach in machine learning.

DNA strand displacement (DSD)^{10,49,50} might provide a viable route for physical realization of our Neural CRN system. The CRNs in the system are primarily non-competitive (NC-CRNs) and are, therefore, catalytic in their reactants. These could be realized through strand displacement frameworks that are optimized towards such reactions, including the enzyme-free “two-domain” strand displacement framework⁵¹ or the strand-displacing polymerase (SDP)-based strand displacement framework.⁴⁷ Furthermore, fast annihilation reactions could be realized via cooperative hybridization complexes.⁵² Time-scale separation between unimolecular and multimolecular reactions could be enforced naturally, as unimolecular reactions could be designed as a single strand displacement reaction, whereas multimolecular reactions typically involve multiple cascaded strand displacements, making them inherently slower. Finally, rate constants can be modulated by both adjusting the strand displacement rates and the fuel complex

concentrations.^{46,47,53}

However, several challenges need to be addressed before we can reliably obtain a practical DSD implementation of the Neural CRNs. The main challenge lies in the implementation of a clock mechanism using oscillatory circuits.^{42,43} DNA circuits in general are susceptible to leaks,^{11,53} which grow exponentially in autocatalytic systems such as oscillators,⁵⁴ presenting a significant implementation challenge. Another challenge involves addressing the issues associated with large-scale DNA circuits, such as crosstalk due to the limited oligonucleotide design space.⁵⁵ Further, the use of dual-rail encoding significantly inflates the circuit size with inactive reactions, presenting an additional obstacle to physical realization. Although, in this work, we showed that the use of dual-rail notation could be significantly reduced through our LR-NCRN system.

Future work on Neural CRNs would involve proposing modifications leveraging the synergy of the framework with the analog chemical computing hardware, such as: (a) discovering alternative hidden state dynamics functions that could potentially reduce the circuit size and implementation complexity; (b) further optimizations to the circuit size through simplifying assumptions (e.g., sparsifying the parameters, first-order approximations of gradients); (c) making the overall system more asynchronous; and (d) extension to multi-class classification (preliminary results in SI Text S9). Furthermore, the system architecture could be easily modified to learn temporal modeling tasks by coupling it with a delay-line circuit or into a reservoir computing system, owing to its dynamical nature. Alternative asymmetric representation of species needs to be explored to avoid the use of dual-rail notation.

5 Methods

The training and inference simulations were performed in Julia (Julia v1.11.3) on an Apple Silicon x64 system. The CRN simulations were performed using the `Catalyst.jl` package using `TRBDF()` as the differential equation solver. For faster experiment repeats, we developed a software tool to generate CRNs by specifying the ODEs in their vector form.¹ The

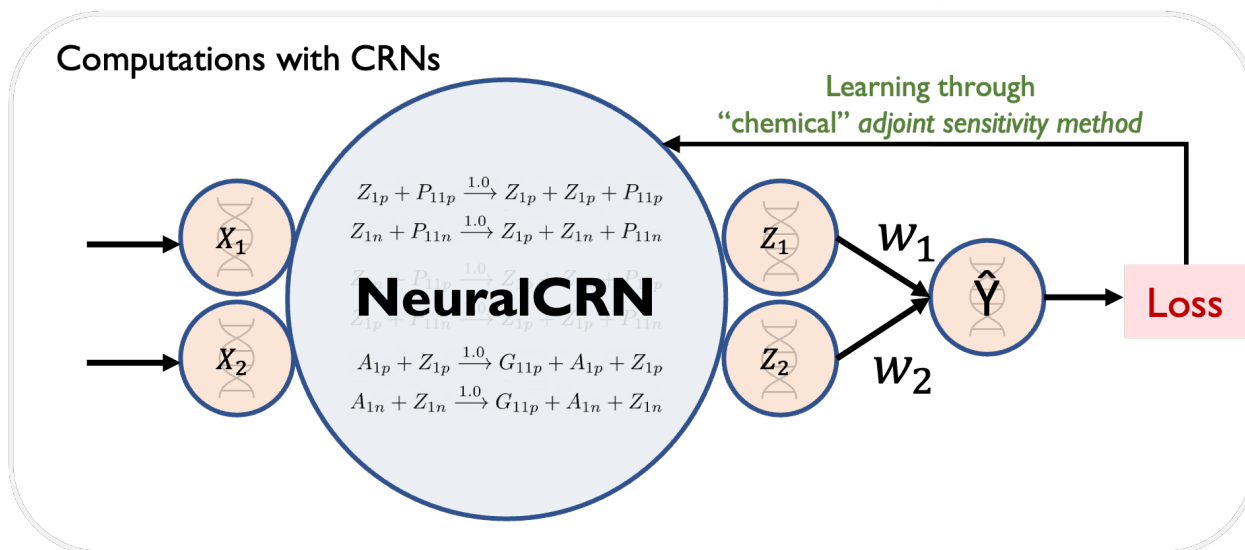
¹Code for the tool

details for the simulation setup of all the demonstration presented in this work are provided in the SI text.

6 Conclusion

In this work, we presented Neural CRNs, a synthetic chemical learning system implemented in deterministic chemical reaction networks. Unlike prior architectures, which chemically mimic the neural network algebras, Neural CRNs employ chemical reactions as I/O devices, leading to concise and simpler reaction systems. The novelty of our approach lies in combining the theory of Neural ODEs^{27,29} with CRN theory³⁰ and stitching them into a chemical learning framework. In this work, we presented a streamlined supervised learning procedure, by first separating the discrete and analog computations in the framework into separate stages and enforcing time-scale separation between them, thereby organizing them within only two clock phases. We then performed several proof-of-concept demonstrations, including linear and nonlinear regression and classification tasks, to validate the supervised learning framework. Notable among these demonstrations include: (a) construction of a minimal-size learning circuit for linear regression, (b) a significant reduction in the circuit size for nonlinear regression through an analog formulation that involves computing approximate gradients, and (c) a nonlinear classifier circuit solely using unimolecular and bimolecular reactions and avoiding trimolecular reactions (previous analog implementations of nonlinearity required trimolecular reactions). Finally, we presented a plausible road map towards a synthetic biochemical implementation of our framework, identifying key design and engineering challenges and proposing possible solutions. Our work introduces a novel paradigm for constructing adaptive biochemical circuits, providing a foundational platform for potential future applications in fields such as synthetic biology, bioengineering, and adaptive biomedicine.

For Table of Contents Only



References

- (1) Koshland, D. E., Jr Special essay. The seven pillars of life. *Science* **2002**, *295*, 2215–2216.
- (2) Webre, D. J.; Wolanin, P. M.; Stock, J. B. Bacterial chemotaxis. *Current Biology* **2003**, *13*, R47–R49.
- (3) Hennessey, T. M.; Rucker, W. B.; McDiarmid, C. G. Classical conditioning in paramecia. *Anim. Learn Behav.* **1979**, *7*, 417–423.
- (4) Jousset, A. Ecological and evolutive implications of bacterial defences against predators. *Environmental microbiology* **2012**, *14*, 1830–1843.
- (5) Lo, E.; Philippidis, G.; Chen, K.-C. Toward A Digestible Biochemical Computer. Proceedings of the Sixth Annual ACM International Conference on Nanoscale Computing and Communication. New York, NY, USA, 2019.
- (6) Zhang, J.; Salaita, K. Smart nucleic acids as future therapeutics. *Trends in Biotechnology* **2021**, *39*, 1289–1307.
- (7) Jones, S. J.; Taylor, A. F.; Beales, P. A. Towards feedback-controlled nanomedicines for smart, adaptive delivery. *Exp. Biol. Med.* **2019**, *244*, 283–293.
- (8) Zhang, C.; Zhao, Y.; Xu, X.; Xu, R.; Li, H.; Teng, X.; Du, Y.; Miao, Y.; Lin, H.-c.; Han, D. Cancer diagnosis with DNA molecular computation. *Nat. Nanotechnol.* **2020**, *15*, 709–715.
- (9) Stano, P. Chemical neural networks and synthetic cell biotechnology: Preludes to chemical AI. International Meeting on Computational Intelligence Methods for Bioinformatics and Biostatistics. 2021; pp 1–12.
- (10) Yurke, B.; Turberfield, A. J.; Mills Jr, A. P.; Simmel, F. C.; Neumann, J. L. A DNA-fuelled molecular machine made of DNA. *Nature* **2000**, *406*, 605–608.
- (11) Zhang, D. Y.; Seelig, G. Dynamic DNA nanotechnology using strand-displacement reactions. *Nat. Chem.* **2011**, *3*, 103–113.

- (12) Qiu, M.; Khisamutdinov, E.; Zhao, Z.; Pan, C.; Choi, J.-W.; Leontis, N. B.; Guo, P. RNA nanotechnology for computer design and in vivo computation. *Philosophical Transactions of the Royal Society A: Mathematical, Physical and Engineering Sciences* **2013**, *371*, 20120310.
- (13) Unger, R.; Moulton, J. Towards computing with proteins. *Proteins: Structure, Function, and Bioinformatics* **2006**, *63*, 53–64.
- (14) Hjelmfelt, A.; Weinberger, E. D.; Ross, J. Chemical implementation of neural networks and Turing machines. *Proc. Natl. Acad. Sci.* **1991**, *88*, 10983–10987.
- (15) Banda, P.; Teuscher, C.; Lakin, M. R. Online learning in a chemical perceptron. *Artif. Life* **2013**, *19*, 195–219.
- (16) Banda, P.; Teuscher, C. In *International Conference on Unconventional Computation and Natural Computation*; Ibarra, O. H., Kari, L., Kopecki, S., Eds.; Springer, 2014; pp 14–26.
- (17) Lakin, M. R.; Minnich, A.; Lane, T.; Stefanovic, D. Design of a biochemical circuit motif for learning linear functions. *J. R. Soc. Interface* **2014**, *11*, 20140902.
- (18) Lakin, M. R.; Stefanovic, D. Supervised Learning in Adaptive DNA Strand Displacement Networks. *ACS Synth. Biol.* **2016**, *5*, 885–897.
- (19) Blount, D.; Banda, P.; Teuscher, C.; Stefanovic, D. Feedforward Chemical Neural Network: An In Silico Chemical System That Learns xor. *Artif. Life* **2017**, *23*, 295–317.
- (20) Arredondo, D.; Lakin, M. R. Supervised Learning in a Multilayer, Nonlinear Chemical Neural Network. *IEEE Trans Neural Netw Learn Syst* **2022**, *PP*.
- (21) Moorman, A.; Samaniego, C. C.; Maley, C.; Weiss, R. A Dynamical Biomolecular Neural Network. 2019 IEEE 58th Conference on Decision and Control (CDC). 2019; pp 1797–1802.

- (22) Vasić, M.; Chalk, C.; Luchsinger, A.; Khurshid, S.; Soloveichik, D. Programming and training rate-independent chemical reaction networks. *Proc. Natl. Acad. Sci. U. S. A.* **2022**, *119*, e2111552119.
- (23) Poole, W.; Ortiz-Munoz, A.; Behera, A.; Jones, N. S.; Ouldrige, T. E.; Winfree, E.; Gopalkrishnan, M. Chemical boltzmann machines. DNA Computing and Molecular Programming: 23rd International Conference, DNA 23, Austin, TX, USA, September 24–28, 2017, Proceedings 23. 2017; pp 210–231.
- (24) Rumelhart, D. E.; Durbin, R.; Golden, R.; Chauvin, Y. *Backpropagation: Theory, Architectures and Applications*; Lawrence Erlbaum Hillsdale, NJ, USA, 1995; pp 1–34.
- (25) Rumelhart, D. E.; Hinton, G. E.; Williams, R. J. Learning representations by back-propagating errors. *Nature* **1986**, *323*, 533–536.
- (26) Rall, L. B. *Automatic differentiation: Techniques and applications*; Springer, 1981.
- (27) Chen, R. T.; Rubanova, Y.; Bettencourt, J.; Duvenaud, D. K. Neural ordinary differential equations. *Advances in neural information processing systems* **2018**, *31*.
- (28) Hairer, E.; Wanner, G. Algebraically stable and implementable Runge-Kutta methods of high order. *SIAM Journal on Numerical Analysis* **1981**, *18*, 1098–1108.
- (29) Pontryagin, L. S. *Mathematical Theory of Optimal Processes*; CRC Press, 1987.
- (30) Hárs, V.; Tóth, J. On the inverse problem of reaction kinetics. *Qualitative theory of differential equations* **1981**, *30*, 363–379.
- (31) Oishi, K.; Klavins, E. Biomolecular implementation of linear I/O systems. *IET Systems Biology* **2011**, *5*, 252–260.
- (32) Cardelli, L.; Tribastone, M.; Tschaikowski, M. From electric circuits to chemical networks. *Nat. Comput.* **2020**, *19*, 237–248.

- (33) Cardelli, L.; Tribastone, M.; Tschaikowski, M.; Vandin, A. Efficient Syntax-Driven Lumping of Differential Equations. *Tools and Algorithms for the Construction and Analysis of Systems*. 2016; pp 93–111.
- (34) Cardelli, L.; Tribastone, M.; Tschaikowski, M.; Vandin, A. Maximal aggregation of polynomial dynamical systems. *Proc. Natl. Acad. Sci. U. S. A.* **2017**, *114*, 10029–10034.
- (35) Dupont, E.; Doucet, A.; Teh, Y. W. Augmented neural odes. *Advances in neural information processing systems* **2019**, *32*.
- (36) Birkhoff, G. D. *Dynamical systems*; American Mathematical Soc., 1927; Vol. 9.
- (37) Mercer, J. Xvi. functions of positive and negative type, and their connection the theory of integral equations. *Philosophical transactions of the royal society of London. Series A, containing papers of a mathematical or physical character* **1909**, *209*, 415–446.
- (38) Rosenblatt, F. The perceptron: a probabilistic model for information storage and organization in the brain. *Psychol. Rev.* **1958**, *65*, 386.
- (39) Anderson, D. F.; Joshi, B.; Deshpande, A. On reaction network implementations of neural networks. *J. R. Soc. Interface* **2021**, *18*, 20210031.
- (40) Vasić, M.; Soloveichik, D.; Khurshid, S. CRN++: Molecular programming language. *Natural Computing* **2020**, *19*, 391–407.
- (41) Jiang, H.; Riedel, M.; Parhi, K. Synchronous sequential computation with molecular reactions. *Proceedings of the 48th Design Automation Conference*. New York, NY, USA, 2011.
- (42) Fujii, T.; Rondelez, Y. Predator–prey molecular ecosystems. *ACS nano* **2013**, *7*, 27–34.
- (43) Srinivas, N.; Parkin, J.; Seelig, G.; Winfree, E.; Soloveichik, D. Enzyme-free nucleic acid dynamical systems. *bioRxiv* **2017**, 138420.

- (44) Jabri, M.; Flower, B. Weight perturbation: An optimal architecture and learning technique for analog VLSI feedforward and recurrent multilayer networks. *IEEE Transactions on Neural Networks* **1992**, *3*, 154–157.
- (45) Hinton, G.; Srivastava, N.; Swersky, K. Neural networks for machine learning lecture 6a overview of mini-batch gradient descent. *Cited on* **2012**, *14*, 2.
- (46) Soloveichik, D.; Seelig, G.; Winfree, E. DNA as a universal substrate for chemical kinetics. *Proc. Natl. Acad. Sci.* **2010**, *107*, 5393–5398.
- (47) Shah, S.; Song, T.; Song, X.; Yang, M.; Reif, J. H. Implementing arbitrary CRNs using strand displacing polymerase. International Conference on DNA Computing and Molecular Programming. 2019; pp 21–36.
- (48) Srivastava, N.; Hinton, G.; Krizhevsky, A.; Sutskever, I.; Salakhutdinov, R. Dropout: a simple way to prevent neural networks from overfitting. *The journal of machine learning research* **2014**, *15*, 1929–1958.
- (49) Lv, H.; Li, Q.; Shi, J.; Fan, C.; Wang, F. Biocomputing based on DNA strand displacement reactions. *ChemPhysChem* **2021**, *22*, 1151–1166.
- (50) Qian, L.; Winfree, E.; Bruck, J. Neural network computation with DNA strand displacement cascades. *Nature* **2011**, *475*, 368–372.
- (51) Cardelli, L. Two-domain DNA strand displacement. *Math. Struct. Comput. Sci.* **2013**, *23*, 247–271.
- (52) Zhang, D. Y. Cooperative hybridization of oligonucleotides. *Journal of the American Chemical Society* **2011**, *133*, 1077–1086.
- (53) Reynaldo, L. P.; Vologodskii, A. V.; Neri, B. P.; Lyamichev, V. I. The kinetics of oligonucleotide replacements. *J. Mol. Biol.* **2000**, *297*, 511–520.
- (54) Nagipogu, R. T.; Reif, J. H. Leak-resilient enzyme-free nucleic acid dynamical systems through shadow cancellation. *Journal of the Royal Society Interface* **2024**, *21*, 20240053.

- (55) Milenkovic, O.; Kashyap, N. On the design of codes for DNA computing. International Workshop on Coding and Cryptography. 2005; pp 100–119.